



## **A compact Scheimpflug lidar imaging instrument for industrial diagnostics of flames**

Downloaded from: <https://research.chalmers.se>, 2025-12-05 04:39 UTC

Citation for the original published paper (version of record):

Dominguez, A., Borggren, J., Xu, C. et al (2023). A compact Scheimpflug lidar imaging instrument for industrial diagnostics of flames. *Measurement Science and Technology*, 34(7).  
<http://dx.doi.org/10.1088/1361-6501/acc268>

N.B. When citing this work, cite the original published paper.

PAPER • OPEN ACCESS

# A compact Scheimpflug lidar imaging instrument for industrial diagnostics of flames



To cite this article: Armand Dominguez *et al* 2023 *Meas. Sci. Technol.* **34** 075901

View the [article online](#) for updates and enhancements.

## You may also like

- [Improvements for volume self-calibration](#)  
Bernhard Wieneke
- [Stereo-particle image velocimetry uncertainty quantification](#)  
Sayantan Bhattacharya, John J Charonko and Pavlos P Vlachos
- [Ionising radiation and lens opacities in interventional physicians: results of a German pilot study](#)  
Ulrike Scheidemann-Wesp, Emilio A L Gianicolo, Rafael J Cámara et al.

# A compact Scheimpflug lidar imaging instrument for industrial diagnostics of flames

Armand Dominguez<sup>1,\*</sup> , Jesper Borggren<sup>2</sup>, Can Xu<sup>2</sup>, Paul Otxoterena<sup>3</sup>, Michael Försth<sup>3,4</sup>, Tomas Leffler<sup>5,6</sup>  and Joakim Bood<sup>1</sup>

<sup>1</sup> Lund University, Div. of Combustion Physics, Box 113, 221 00 Lund, Sweden

<sup>2</sup> Beamonics AB, Tellusgatan 13, 224 57 Lund, Sweden

<sup>3</sup> RISE Research Institutes of Sweden, Box 857, 501 15 Borås, Sweden

<sup>4</sup> Luleå University of Technology, Department of Civil, Environmental and Natural Resources Engineering, 971 87 Luleå, Sweden

<sup>5</sup> Vattenfall AB, Laboratorievägen, 814 26 Älvkarleby, Sweden

<sup>6</sup> Chalmers, Chemistry and Chemical Engineering, 412 96 Göteborg, Sweden

E-mail: [armand\\_bastian.dominguez@forbrf.lth.se](mailto:armand_bastian.dominguez@forbrf.lth.se)

Received 21 November 2022, revised 27 February 2023

Accepted for publication 8 March 2023

Published 30 March 2023



## Abstract

Scheimpflug lidar is a compact alternative to traditional lidar setups. With Scheimpflug lidar it is possible to make continuous range-resolved measurements. In this study we investigate the feasibility of a Scheimpflug lidar instrument for remote sensing in pool flames, which are characterized by strong particle scattering, large temperature gradients, and substantial fluctuations in particle distribution due to turbulence. An extinction coefficient can be extracted using the information about the transmitted laser power and the spatial extent of the flame. The transmitted laser power is manifested by the intensity of the ‘echo’ from a hard-target termination of the beam located behind the flame, while the information of the spatial extent of the flame along the laser beam is provided by the range-resolved scattering signal. Measurements were performed in heptane and diesel flames, respectively.

Keywords: lidar, real-time monitoring, combustion

(Some figures may appear in colour only in the online journal)

## 1. Introduction

Light detection and ranging (lidar), is an optical remote sensing technique in which backscattered light from a laser beam is detected with range resolution. The well-defined spatial, temporal, and spectral properties of laser light allow a lidar system

to provide information about a probe volume extending over distances in the order of kilometers. The technique is well established in atmospheric science, where it is applied to monitor and characterize temperature, wind speed, and atomic/molecular and particulate species [1–3]. In addition to atmospheric science, other application fields include topography, forestry, and ecological research [4–6]. The principles of lidar and examples of applications are described in [7, 8].

Although lidar technology has changed since its advent in the 1970s, the design has remained mostly constant; a high-intensity laser pulse of short duration (typically 10 ns) transects a remote region of interest, and the induced light scattering is collected by a telescope and temporally resolved

\* Author to whom any correspondence should be addressed.



Original content from this work may be used under the terms of the [Creative Commons Attribution 4.0 licence](https://creativecommons.org/licenses/by/4.0/). Any further distribution of this work must maintain attribution to the author(s) and the title of the work, journal citation and DOI.

on a detector. Range-resolved information is hence readily obtained by converting the time-resolved signal into a range-resolved signal using the speed of light in the medium. Ultimately, the range resolution,  $\Delta R = c\tau_L/2$ , is limited by the laser pulse duration  $L$ . Nanosecond laser pulses thus provide a maximum range resolution of approximately 1 m, which is adequate in many applications, but often insufficient for industrial combustion studies, such as monitoring processes in power plants, boilers, or fires. The range resolution can be improved by using shorter laser pulses as long as the detector provides a bandwidth that matches the laser pulse duration. A range resolution of 5 mm has been demonstrated using a picosecond laser and a streak camera [9]. The ps-lidar system was demonstrated for thermometry in a full-scale room fire experiment [10]. Despite the potential for ps-lidar, it requires a heavy and bulky system and a mode-locked picosecond laser, which also necessitates quite stable conditions in terms of the temperature and humidity of the surroundings. On-site industrial applications are therefore very challenging.

In 2015, a new lidar technique was proposed and demonstrated [11]. This technique, called Scheimpflug-lidar, does not utilize the time-of-flight concept, but rather achieves range resolution by imaging the backscattered light onto a tilted linear sensor. In a sense, this approach is reminiscent of the very first attempts at active remote sensing based on triangulation with continuous-wave (cw) searchlights. Scheimpflug-lidar requires a setup aligned so that the laser beam, the optical axis of the collection optics, and the orientation of the linear sensor satisfy the Scheimpflug condition. Correctly aligned, the focal plane of the sensor is located along the laser beam and thus the scattered laser light can be sharply imaged with spatial resolution along the laser beam propagation direction. Since the technique does not require a high-power short-pulse laser, the setup is compact and relatively inexpensive due to the availability of cw diode lasers. Since the first demonstration of the technique for atmospheric sensing of oxygen concentration based on differential absorption [11], it has been applied, primarily, in ecological research [6]. Furthermore, down-sized setups suitable for combustion diagnostics have been demonstrated [3, 12].

In the present work a prototype for a compact and portable Scheimpflug-lidar instrument has been designed and its feasibility for practical applications in full-scale industrial environments has been tested. The lidar device contains both light source (a 40 mW cw diode laser) and collection optics in a single unit mounted on a tripod, and instrumental settings and data acquisition are controlled by a laptop PC. The measurements were performed in pool fires (turbulent diffusion flames) created by burning evaporating liquid fuels contained in a 60 cm diameter pool. The sooty pool fires were located about 3 m from the lidar device. Flames based on two different fuels, namely heptane and diesel, were investigated. The study demonstrates that the total flame extinction can be determined quantitatively by analyzing the intensity of the lidar signal reflected off a beam termination screen located about 4 m behind the flame. The simultaneously recorded range-resolved scattering signal from the flame allows estimation of the flame size along the laser beam direction, and

dividing by the measured total extinction yields an extinction coefficient. The results show that the lidar device is feasible for remote sensing in larger combustion environments, which is promising for applications in full-scale industrial environments, where conditions are harsh and optical access is limited.

## 2. Methods and materials

Figure 1 shows a photograph of the lidar instrument mounted on a tripod. The device has the dimensions  $50 \times 40 \times 20 \text{ cm}^3$ , and weighs about 13 kg. With the tripod set up and extended, the device stands at 1 m. Due to its smaller size and compactibility, the lidar instrument can fit into the trunk of a regular passenger car, thus allowing easy transportation. Preparation of the system prior to a field experiment takes about 30 min to an hour for the first initialization. To initialize the setup, first, theoretical calculations are made to determine the location of where the lidar device should be placed for the observed area. Once the lidar device is placed in its position, a rough alignment is done by observing the back-reflected light on the diode array. Afterwards, the signal can be observed on the computer and the angle of the laser can be changed to optimize the signal and place the back reflection of a known distance at a specific pixel. Additional changes to the lens and sensor focusing are done to further optimize the signal. Once the setup has been aligned, further adjustments can be made within minutes to optimize the signal.

Figure 2 shows a schematic illustration of the optical arrangement for Scheimpflug lidar. As can be seen, the detector, i.e. a line-array CMOS sensor (Hamamatsu, S11639-01, 2048 pixels), is tilted relative to the collection lens (2" diameter). The intersection of the image plane, in which the line-array detector is located, the lens plane, and the object plane, in which the laser beam is propagating, is called the Scheimpflug intersection. In addition, the position of the object plane is constrained by the Hinge rule, which dictates that the front focal plane of the lens, the object plane, and the image plane displaced to the center of the lens, must coincide.

With the system aligned according to the mentioned principles, the 450 nm diffraction-limited cw laser beam, provided by a diode laser (Thorlabs PL450B-450 nm, 80 mW maximum output power, 100:1 linear polarization), a section of the beam, corresponding to the start of the field of view (red star) to a point corresponding to the end of the field of view (green circle), is sharply imaged onto the line-array sensor.

The angle of viewing constrains the resolution and results in a nonlinear range resolution i.e. a pixel receiving light from a far location accommodates light from a longer sample volume than a pixel receiving light from a nearby location. A consequence of the resolution varying nonlinearly with range is that it counteracts the inevitable  $1/R^2$  dependence of the light collection efficiency, meaning that it is possible to obtain an instrument response that is essentially constant across the entire range, thus maximizing the dynamic range of the instrument [12]. In order to suppress light at other wavelengths than 450 nm, an interference filter, having center transmission wavelength at 450 nm and 10 nm full width at



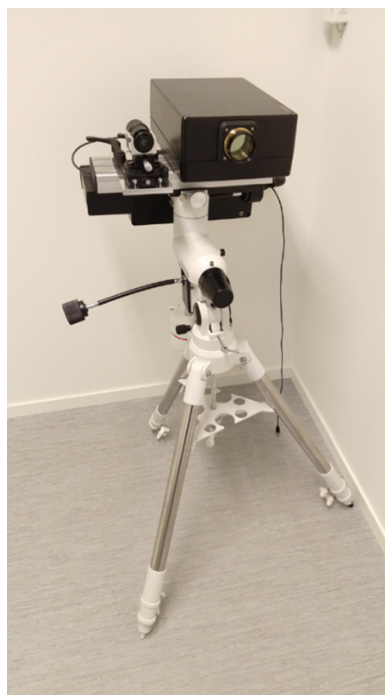


Figure 1. Photography of the Scheimpflug-lidar device.

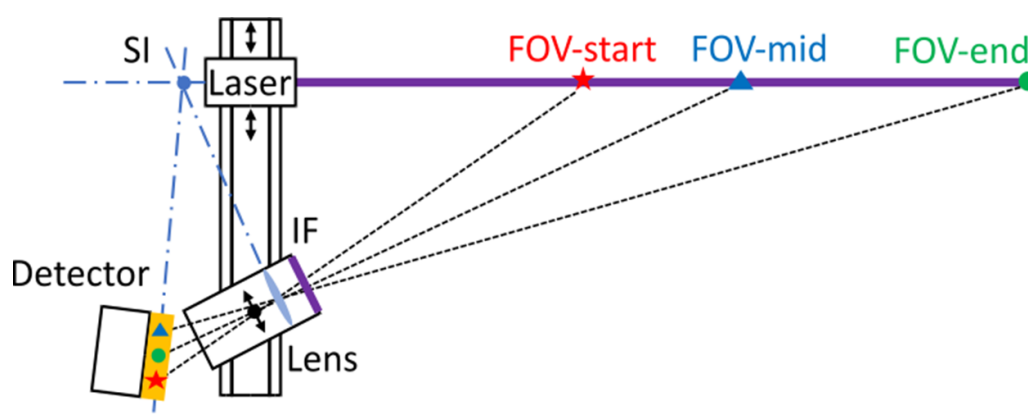


Figure 2. Schematic illustration of the optical arrangement for Scheimpflug-lidar.

half maximum (FWHM), is positioned in front of the collection lens. Data acquisition and instrument settings are controlled by a laptop PC. The lidar instrument not only provides high range resolution, but also high temporal resolution, as the line-array detector has a maximum effective sampling rate of  $2000 \text{ lines s}^{-1}$  and 16-bit dynamic range, allowing for studies of the dynamics of large probe volumes. The high sampling rate of the line-array detector also offers online background subtraction by modulating the laser beam on and off in synchronization with the detector exposures [4].

In the present experiments, the laser beam is directed towards a termination screen located about 7 m from the lidar instrument. Between the instrument and the termination screen a pool flame is positioned, at a distance of about 3 m from the lidar instrument. The flame is produced by igniting the liquid fuel inside a 0.6 m diameter pool (see the photo in figure 3).

### 3. Results and discussion

Figure 4 shows sets of lidar data recorded in a heptane flame (panel a) and a diesel flame (panel b), respectively, with a laser power of 40 mW. A background, corresponding to the signal recorded with the laser beam switched off, was subtracted according to the on-line subtraction procedure described above. The heptane flame data (panel a) was recorded with a sampling rate of  $1000 \text{ lines s}^{-1}$ , whereas the diesel flame data was recorded with a rate of  $2000 \text{ lines s}^{-1}$ . In the data matrices, time is on the  $x$ -axis, range (distance from the lidar device) is on the  $y$ -axis, while the color scale reflects lidar signal intensity. Each column is a lidar curve recorded at a particular time. Note that the  $x$ -scale and the color bars are different in the two panels. A bright band located at a distance of  $\sim 3 \text{ m}$  is clearly observable in panel a. This band corresponds to



**Figure 3.** Photo of the experiment. The lidar device located in the lower left portion of the photo is aimed at the flame. The laser beam passes through the flame, giving rise to strong elastic light scattering, and is then terminated on a screen located behind the flame.

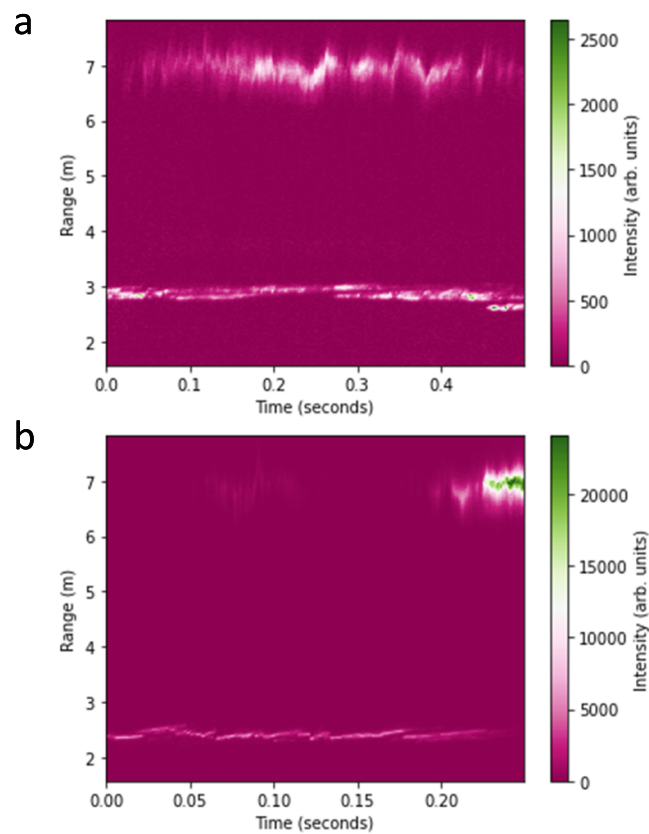


**Figure 4.** Lidar data recorded from the heptane flame (a) and diesel flame (b). Note the different x- and color scales.

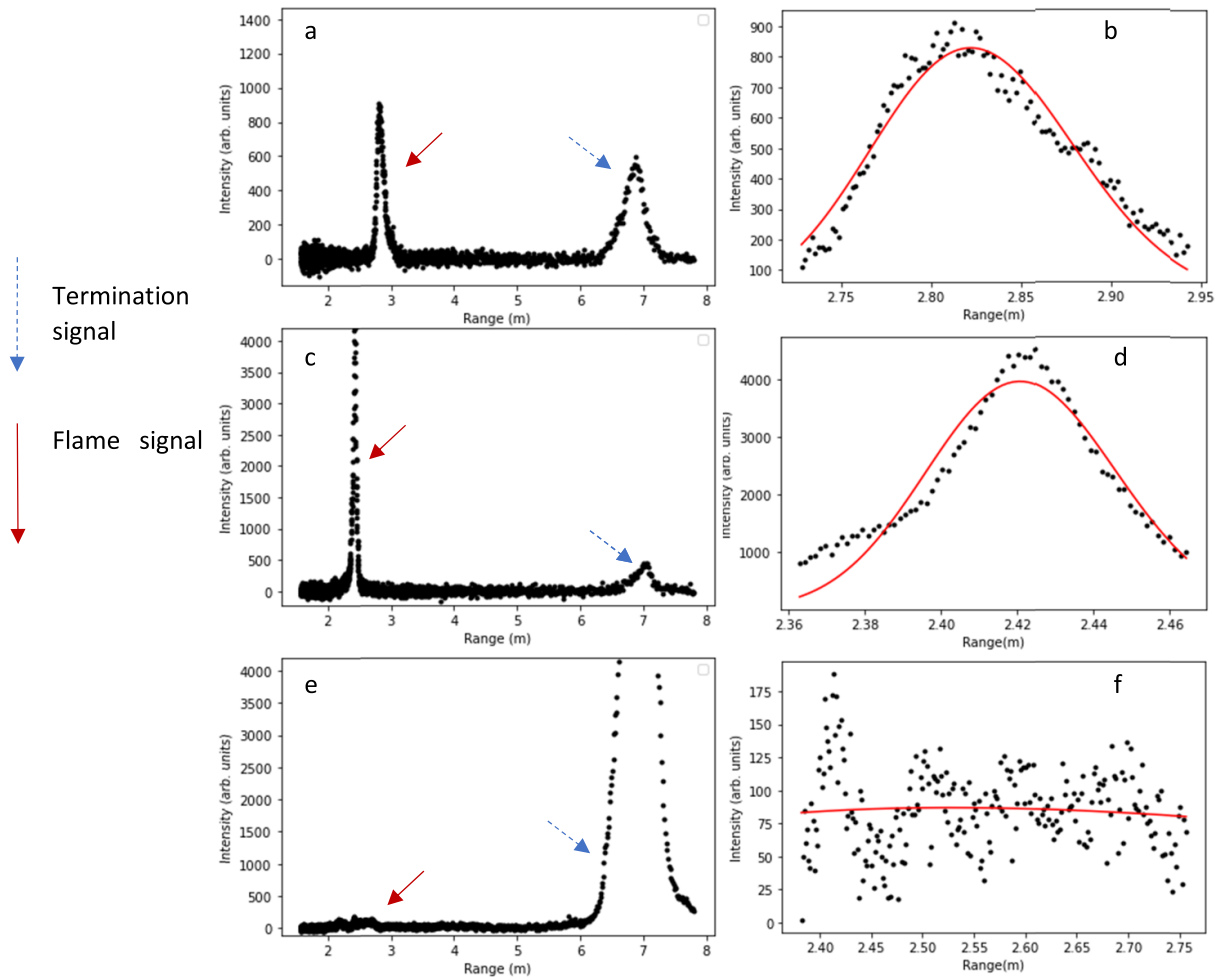


**Figure 5.** (a) Example of a single lidar curve extracted from the data shown in figure 4(a). (b) The signal due to scattering from the flame (dots) together with the best-fit Gaussian profile (solid red line). (c) Example of single lidar curve extracted from data shown in figure 4(b). (d) The signal due to scattering from the flame (dots) together with the best-fit Gaussian profile (solid red line). (e) Example of single lidar curve from figure 4(b) when the diesel flame is dying and no longer acts as single flame. (f) Poorly fitted Gaussian fit to dying flame in figure 5(e).

elastic scattering from the flame. From the color bar it is evident that the scattering signal from the diesel flame (panel b) is significantly stronger than the scattering from the heptane flame (panel a).

The other bright structure, at a distance of  $\sim 7$  m corresponds to laser light reflected off of the termination screen. The intensity and the position of the termination signal varies over time. The variation in intensity is due to the varying scattering of the turbulent flame, i.e. the extinction of the laser light varies in time. This relation between extinction observed through the strength of the termination ‘echo’ and the light scattering caused by the flame is particularly evident at the time 0.22 s in panel b, where the flame is abruptly extinguished, thus resulting in an abrupt increase in the termination signal intensity. The reason for the spatial variation of the termination signal over time observed in both panels is most likely beam steering from flame turbulence.

Examples of single lidar curves, extracted from the data displayed in figure 4, are shown in figure 5. The scattering from the flame is evident as a distinct peak located at about 3 m away for the heptane flame and about 2.5 m for the diesel flame.

The reflection from the termination screen corresponds to the intense peak at about 7 m distance. It is possible to estimate the spatial extent of the flame along the laser beam direction by fitting a Gaussian function to the scattering signal from the flame, as shown in figures 5(b) and (d). This method is limited by the shape of the flame and an example of when this method no longer applies can be seen in figure 5(e), where the application of a Gaussian fit to the flame gives the result in figure 5(f). Regardless of the poor fit, the lidar curve still gives spatial information and merely requires a more robust and complicated method to extract more precise spatial information from a non-Gaussian shape. The  $S/N$  ratio is measured by taking the ratio between the noise (defined as the rms value) located outside of the signals and the peak height of the Gaussian as shown in figure 5(b) gives a  $S/N$  of 31.9 while the  $S/N$  corresponding to the data shown in figures 5(d) and (f) are 82.3 and 3.29, respectively. Taking all the  $S/N$  ratio of all the lidar curves in figures 4(a) and (b) give an average  $S/N$  ratio of 32.3 for the heptane flame and 86.5 for the diesel flame.

Taking the FWHM as the flame size, figure 6 shows the measured flame size for the heptane flame (panel a) and the

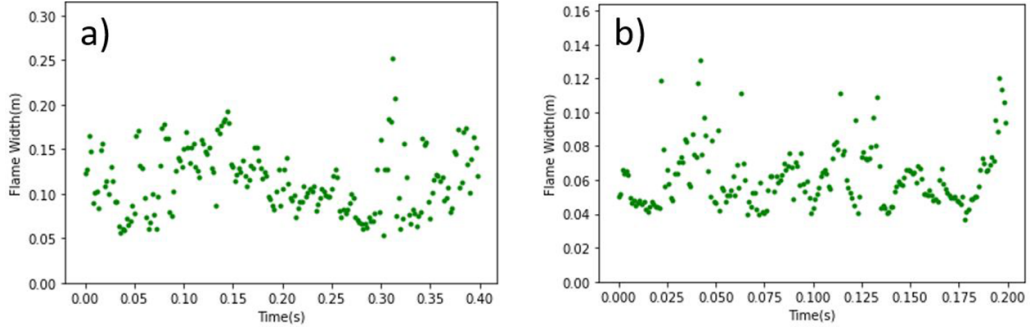


**Figure 6.** Measured flame size along the laser beam for the heptane (a) and diesel flame (b).

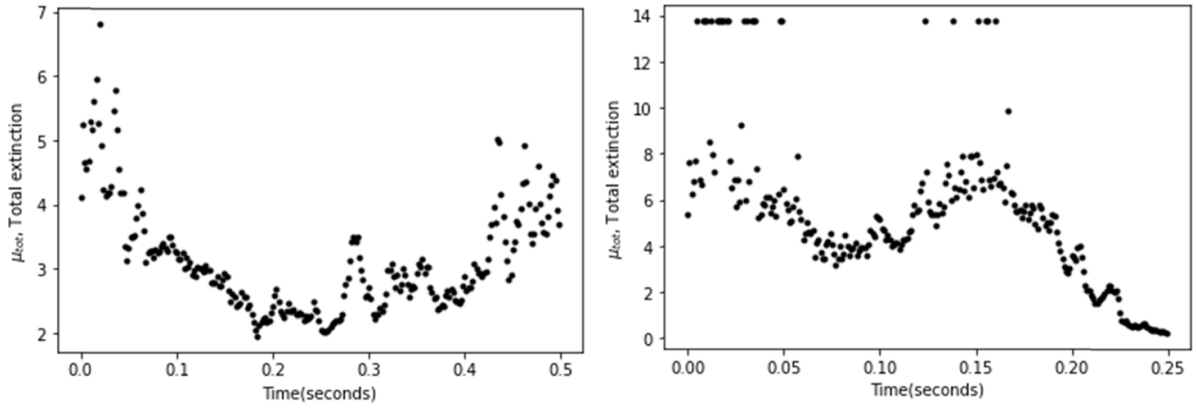


**Figure 7.** Measured total extinction for the heptane (a) and diesel flame (b), respectively.

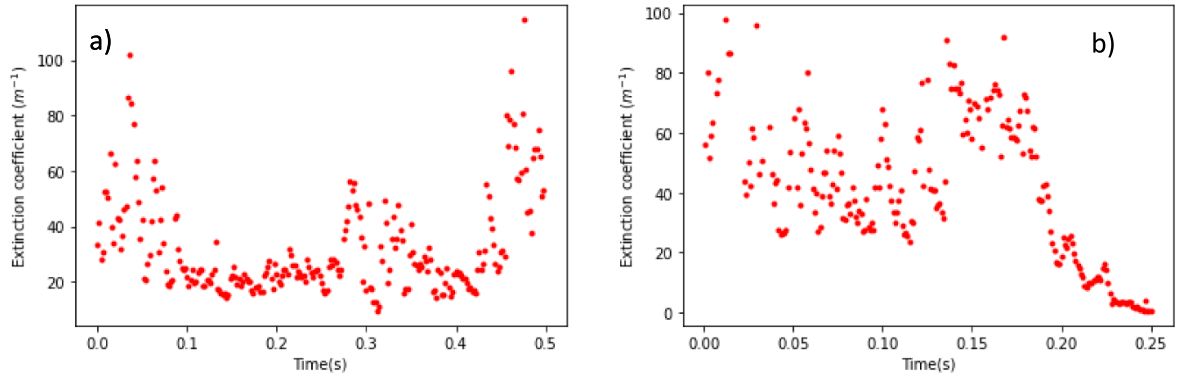


**Figure 8.** Measured extinction coefficients for the heptane (a) and diesel flame (b).

diesel flame (panel b). The mean flame size for the heptane flame is 0.11 m and the standard deviation is 0.040 m. The diesel flame size is a little more than half as large, with a mean value of 0.07 m and a standard deviation 0.05 m.

The total flame extinction can be extracted from the intensity of the peak due to the reflection from the termination screen. The reference intensity,  $I_0$ , (corresponding to zero extinction) is the termination peak intensity recorded without a flame. Hence, with a termination peak intensity recorded with the flame present,  $I_f$ , the total extinction is given by

$$\mu_{\text{tot}} = \ln \frac{I_0}{I_f}. \quad (1)$$

Next, the flame-size results, shown in figure 6, are combined with the measured total extinction, shown in figure 7, to extract an extinction coefficient, which is given by

$$\mu = \frac{\mu_{\text{tot}}}{L_{\text{flame}}} \quad (2)$$

where  $L_{\text{flame}}$  is the flame size as defined above. The evaluated extinction coefficients for the two flames are plotted in figure 8. The mean extinction coefficient is  $33 \text{ m}^{-1}$  (standard deviation  $18 \text{ m}^{-1}$ ) for the heptane flame and  $96 \text{ m}^{-1}$  (standard deviation  $72 \text{ m}^{-1}$ ) for the diesel flame. The extinction coefficient for the diesel flame is about three times

higher than for the heptane flame. This result is not surprising since a diffusion flame burning on diesel gives rise to higher soot volume fraction than a flame burning on heptane [13]. The standard deviations of the extinction coefficients suggest that the combustion of diesel is more turbulent than for heptane.

#### 4. Conclusions

A compact and portable lidar instrument, based on the Scheimpflug principle, has been constructed and its feasibility for practical diagnostics has been investigated through remote sensing experiments on pool fires burning heptane and diesel. Overall, the experiments demonstrate that the instrument withstands the prevailing challenging conditions, i.e. variations in temperature and humidity. By combining the information of the laser light transmission through the flame, achieved via the intensity of the laser light reflected off a termination screen, and the spatial extent of the flame, obtained through the range resolved flame scattering, extinction coefficients for the flames can be estimated. These results indicate that the Scheimpflug lidar device, requiring only one optical port and providing range-resolved remote sensing, could be a valuable diagnostic tool in harsh intractable environments such as those prevailing in real industrial applications.

#### Data availability statement

The data that support the findings of this study are available upon reasonable request from the authors.

#### Acknowledgments

This project was supported by research Grants from Swedish Governmental Agency for Innovation Systems, Vinnova (Smartare Elektroniksystem, Project Number 2018-01551) and the Swedish Foundation for Strategic Research (SSF) through Project Number TM17-0309.

#### Conflict of interest

We have no known conflict of interest to report.

#### ORCID iDs

Armand Dominguez  <https://orcid.org/0000-0002-3527-9262>

Tomas Leffler  <https://orcid.org/0000-0002-4374-9690>

#### References

- [1] Arshinov Y F, Bobrovnikov S M, Zuev V E and Mitev V M 1983 Atmospheric temperature measurements using a pure rotational Raman lidar *Appl. Opt.* **22** 2984–90
- [2] Hu Y *et al* 2008 Sea surface wind speed estimation from space based lidar measurements *Atmospheric Chem. Phys.* **8** 3593–601
- [3] Bood J 2019 Lidar thermometry using two-line atomic fluorescence *Appl. Opt.* **58** 1128
- [4] Mei L and Brydegaard M 2015 Atmospheric aerosol monitoring by an elastic Scheimpflug lidar system *Opt. Express* **23** A1613
- [5] Wang X, Pan H, Guo K, Yang X and Luo S 2020 The evolution of lidar and its application in high precision measurement *IOP Conf. Ser.: Earth Environ. Sci.* **502** 012008
- [6] Malmqvist E *et al* 2018 The bat-bird-bug battle: daily flight activity of insects and their predators over a rice field revealed by high-resolution Scheimpflug lidar *R. Soc. Open Sci.* **5**
- [7] Brydegaard M, Malmqvist E, Jansson S, Larsson J, Török S and Zhao G 2017 The Scheimpflug lidar method *Proc. SPIE* **10406**
- [8] Theodor Scheimpflug T S 1904 Method of distorting plane images by means of lenses or mirrors (US751347A) *USPTO* (available at: <https://patents.google.com/patent/US751347A/en>)
- [9] Kaldvee B, Ehn A, Bood J and Aldén M 2009 Development of a picosecond lidar system for large-scale combustion diagnostics *Appl. Opt.* **48** B65–B72
- [10] Kaldvee B, Wahlqvist J, Jonsson M, Brackmann C, Andersson B, van Hees P, Bood J and Aldén M 2013 Room-fire characterization using highly range-resolved picosecond lidar diagnostics and CFD simulations *Combust. Sci. Technol.* **185** 749–65
- [11] Mei L and Brydegaard M 2015 Continuous-wave differential absorption lidar *Laser Photonics Rev.* **9** 629–36
- [12] Malmqvist E, Brydegaard M, Aldén M and Bood J 2018 Scheimpflug lidar for combustion diagnostics *Opt. Express* **26** 14842–58
- [13] Colbeck I, Atkinson B and Johar Y 1997 The morphology and optical properties of soot produced by different fuels *J. Aerosol Sci.* **28** 715–23